Adsorption 2, 193–203 (1996)

Adsorption and Selectivity of Carbon Dioxide with Methane and Nitrogen in Slit-Shaped Carbonaceous Micropores: Simulation and Experiment

ROGER F. CRACKNELL AND DAVID NICHOLSON
Department of Chemistry, Imperial College of Science, Technology and Medicine, London SW72AY

STEPHEN R. TENNISON* AND JILL BROMHEAD
BP Sunbury Research Centre, Chertsey Rd, Sunbury on Thames, Middlesex TW167LN

Received July 27, 1995; Revised November 22, 1995; Accepted December 7, 1995

Abstract. We have used the grand canonical Monte Carlo method to study the adsorption and selectivity of mixtures of carbon dioxide with methane and nitrogen at high (i.e., ambient) temperatures in model slit pores with graphitic surfaces. Experimental data, including new high pressure measurements for carbon dioxide and methane on a non-porous graphitic standard, were used to test the potential models. The mixture simulations predict that carbon dioxide is preferentially adsorbed in both systems. The results are discussed in terms of competing energetic and entropic effects and the underlying molecular mechanisms.

Keywords: mixture adsorption, cabon dioxide, methane, carbon pores, simulation

Introduction

Carbon dioxide has been implicated as a greenhouse gas, the atmospheric emission of which may cause global warming. The Climate Change Convention signed at the Earth Summit at Rio de Janeiro in June 1992 encourages (but does not require) nations to stabilise emissions of greenhouse gases at 1990 levels by 2000. Whatever the validity of the scientific arguments concerning global warming, the threat of a future international treaty compelling control of CO_2 emissions provides an economic incentive for the development of cheap and efficient methods for separating CO_2 from gas mixtures.

Gas mixtures can be separated cryogenically (i.e., liquefaction of the mixture, followed by distillation of each component) or alternatively by selective adsorption of one species in a microporous material. Keller (1983) has discussed the factors which make one method preferable to another; the most important criterion being the effectiveness of the separation. For adsorptive separation of CO_2 from a binary mixture, the effectiveness can be quantified in terms of the selectivity (or separation factor) S, defined as

$$S = \frac{x_{CO_2}/x_i}{y_{CO_2}/y_i} \tag{1}$$

where x_{CO_2} and x_i are the mole fractions of the carbon dioxide and the coadsorbed gas in the micropore and y_{CO_2} and y_i the corresponding mole fractions in the external equilibrium gas phase.

The grand canonical Monte Carlo (GCMC) technique has been used to simulate mixture adsorption in zeolites (Karavias and Myers, 1991; Razmus and Hall, 1991; Maddox and Rowlinson, 1993; Van Tassel et al., 1994) heterogeneous silica pores (Kaminsky and Monson, 1994), mica slits (Somers et al., 1993), and graphitic slit pores (Cracknell et al., 1993, 1994; Cracknell and Nicholson, 1994, 1995). Various mean field density functional theories (MFDFT) have also

*Present address: Materials and Separations Technology Int. Ltd. Addlestone, Surrey KT15 3HR, UK.

been used to probe the way in which selectivity varies with pressure for a number of model systems (Tan et al., 1989; Kierlik and Rosinberg, 1991; Tan and Gubbins, 1992; Jiang et al., 1994). Although generally less accurate than the Monte Carlo techniques, MFDFT approaches are less computationally demanding. The present work is part of a series of publications concerned with optimising gas separation in microporous activated carbon materials, in all cases the micropores in the carbons have been assumed to have a slit geometry. In the first paper (Cracknell et al., 1993) both methane and ethane were modelled as Lennard-Jones spheres in order to compare the GCMC method and the MFDFT calculations of Tan and Gubbins (1992) on the same system. In the following paper (Cracknell et al., 1994) ethane was modelled using a two-centre Lennard Jones potential; the non sphericity of the ethane molecule was found to have a profound influence on the variation of selectivity with both bulk pressure and pore width. A multicentre model of ethane propane mixtures has also been studied (Cracknell and Nicholson, 1994).

In the only previous simulation study of carbon dioxide as part of a binary adsorbed mixture (Karavias and Myers, 1991) the molecule was modelled as a Lennard-Jones sphere with a quadrupole. However our previous results (Cracknell et al., 1994; Cracknell and Nicholson, 1994) suggest that molecular shape can be expected to have a significant influence on the properties of an adsorbed mixture. In the molecular dynamics simulation by Hammonds et al. (1990) of CO_2 adsorption at low temperatures on a single graphite surface various models for CO_2 were used. Here we compare simulated adsorption isotherms for two models of CO_2 on a graphite surface with new experimental high pressure adsorption measurements on a non-porous carbon. Models for nitrogen and methane have been established in previous work. We use these models to study the adsorption of mixtures of these gases with CO_2 in model carbon pores. A motivation for this study comes from the interest in developing a membrane process for CO_2 separations. For example, many gas fields, particularly those in the Pacific basin, contain large amounts of CO_2 (up to 70%). This must be removed and reinjected into the wells to achieve the required calorific value. This is at present uneconomical because of the very high capital and energy cost of recompressing the CO_2 to the well head pressure which may be as much as 100 bar.

Grand Canonical Monte Carlo Method

Adsorption simulations were carried out using the grand canonical Monte Carlo technique. For single component simulations, three types of trial were used: attempts to move particles, attempts to delete particles, and attempts to create particles. Microscopic reversibility requires that an equal number of creation and deletion attempts be made. In a move attempt, one particle is chosen at random from those in the simulation and given a random displacement (and rotation for a non-spherical particle); the new configuration is accepted with a probability

$$P_{\mathrm{MOV}}^{\mathrm{ACC}} = \min[1, \exp(-\beta \Delta E_c)] \tag{2}$$

where ΔE_c is the change in configurational energy resulting from the trial. The maximum amount by which the particle was displaced (and rotated) was adjusted to give an acceptance rate of approximately 50%. For a creation attempt, a position and orientation are chosen at random, and the new particle accepted with probability

$$P_{\mathrm{CR}}^{\mathrm{ACC}} = \min\left[1, \frac{z_i V}{N_i + 1} \exp(-\beta \Delta E_c)\right] \tag{3}$$

where V is the volume of the system, and N_i, is the number of particles of component i in the system (prior to the creation attempt). The absolute activity, z_i is given by

$$z_i = \frac{\exp(\beta \mu_i)}{\Lambda_{t,i}^3 \Lambda_{r,i}} \tag{4}$$

where μ_i is the chemical potential of component i, $\Lambda_{t,i}$ is the reciprocal of the translational molecular partition function for i in one dimension, and $\Lambda_{r,i}$ is the reciprocal of the rotational partition function of i. To ensure a random orientation of the particle for insertion trials, we used the algorithm due to Marsaglia described in Allen and Tildesley (1987) which generates random points on the surface of a sphere.

For an attempted deletion, a particle was chosen from the system at random and deleted with probability.

$$P_{\mathrm{DEL}}^{\mathrm{ACC}} = \min\left[1, \frac{N_i}{z_i V} \exp(-\beta \Delta E_c)\right] \tag{5}$$

For mixture simulations, an additional type of trial was employed, in which attempts were made to interchange the identities of particles. To change the identity of a

particle of type i into type j, a particle of type i is chosen at random and the identity change is accepted with probability

$$P_{i\to j}^{\mathrm{ACC}} = \min\left[1, \frac{z_j N_i}{z_i(N_j+1)} \exp(-\beta \Delta E_c)\right] \quad (6)$$

Identity changes from j to i are given by the expression of (6) with the subscripts interchanged. Microscopic reversibility requires that an identical number of i to j swaps be attempted as j to i. GCMC simulations of mixtures can be conducted without particle exchange trials, however employing exchanges leads to greatly improved statistics for the calculation of separation factors in the simulation (Kofke, 1991; Cracknell et al., 1993).

To calculate adsorption isotherms, simulations were conducted corresponding to various values of z_i for a single component simulation and z_i and z_j for a mixture simulation. These parameters were then related to bulk phase pressures and mole fractions by using either the ideal gas law relation,

$$P_i = z_i kT \quad (7)$$

or by running a GCMC simulation of a bulk gas and using the virial theorem to calculate the pressures. The simulations were run for 5×10^6 configurations on "Intel i860" processors in a Transtech "parastation" with a 486 PC acting as host. The simulations took between 4–6 hours to run depending on the number of particles in the system which was typically between 200 and 300.

High Pressure Adsorption Measurements

Methane and carbon dioxide adsorption isotherms at 313 K were measured on Vulcan 3G (2700), a graphitised carbon black certified reference material from the National Physical Laboratory UK; sample number 2A/1/E/4, surface area 77.3 m^2g^{-1} (Everett et al., 1974), using a high pressure balance. A schematic diagram of the experimental apparatus is shown in Fig. 1. A 4406MP8 Sartorius balance was mounted onto a frame placed on a floor-mounted, vibrationally stabilised, platform. An accurately controlled fan oven was built around the balance such that it was not in contact with the platform and could not transmit vibration to the balance. The oven had an upper temperature limit of 80 C, which was the maximum

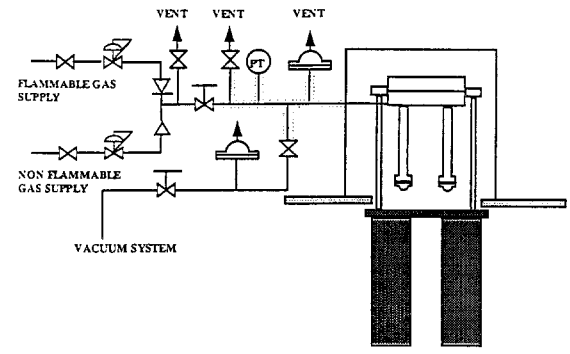

Figure 1. High pressure adsorption rig.

operating temperature of the balance. All parts of the gas pipework external to the oven but directly connected to the balance during operation were trace heated. The vacuum system comprised an Edwards E2M2 rotary pump and an Edwards diffstak 63/150 connected in series, with an alumina foreline trap. The vacuum achieved in the sample chamber was not accurately measured since it was expected to be lower than that measured at the pump head.

The balance system employed on-line data logging and was capable of operating up to 70 bar with either flammable or non-flammable adsorptives. Methane and carbon dioxide isotherms were determined on fresh samples of the adsorbent. Sample weights of 0.5 to 0.7 g were used, the sample was desorbed at 80 C under full vacuum to constant weight. No counter weight was used for the sample; the hangdown wires and glass sample buckets on the weighing and tare sides were adjusted to be as nearly as possible balanced. Buoyancy corrections were calculated for each isotherm point by calculating the volume of gas displaced by the sample from its helium density (1.92 gcm^{-3}) and its desorbed weight. The molar volume of the gas under the experimental conditions was then calculated from the Peng Robinson equation of state and hence the weight of the gas was calculated.

Intermolecular Potentials

Adsorbate-Adsorbent Interactions

The micropore was modelled as the cavity between two walls of parallel stacked graphite planes extending to infinity. The pore width, H, is the distance between carbon centres on the opposite wall of the micropore. A real microporous activated carbon is likely to be

composed of pores of various widths, thus making the adsorbent energetically heterogeneous, although recently certain activated carbon fibres have been shown to have a very narrow pore size distribution (Kaneko et al., 1992) having pore shapes consistent with the slit model.

The dispersion interaction energy between a site on a gas molecule and a single graphite surface, as a function of the distance z from it, is given by the 10-4-3 potential of Steele (1974)

$$u_{sf}(z) = 2\pi\rho_s\epsilon_{sf}\sigma_{sf}^2\Delta\left[\frac{2}{5}\left(\frac{\sigma_{sf}}{z}\right)^{10} - \left(\frac{\sigma_{sf}}{z}\right)^4 - \frac{\sigma_{sf}^4}{3\Delta(0.61\Delta + z)^3}\right] \quad (8)$$

where Δ is the separation between graphite layers (=0.335 nm) and ρ_s is the number density of carbon atoms in a graphite (114 nm^{-3}). σ_{sf} and ε_{sf} are the solid-fluid Lennard-Jones parameters which were calculated by combining the graphite parameters ($\sigma_{ss} = 0.340$ nm, $\varepsilon_{ss}/k = 28.0$ K[24]) with the appropriate parameters for the gas using the Lorentz-Berthelot rules. The external field, $u_{sf}^{(1)}$, in a slit pore of width H is the sum of the interaction with both graphitic surfaces and can be expressed mathematically as

$$u_{sf}^{(1)} = u_{sf}(z) + u_{sf}(H - z) \quad (9)$$

Equation (9) ignores the surface corrugation, which is unlikely to significantly affect the results at ambient temperatures.

The models for CO_2 and N_2 that were adopted (see below) use point charges to model the permanent quadrupole on each molecule. The permanent charge distribution on each molecule will in reality polarize the surface so there will be an additional quadrupole-induced quadrupole contribution to the gas surface potential. We did not include this effect in our calculations. Firstly because calculations showed it to make a relatively small contribution to the gas-solid energy (<1%) and we were able to get good agreement with experimental isotherms for a single surface without this contribution (see below). Secondly there is ambiguity in deciding where to place the electrostatic image plane in the graphite surface (Hammonds et al., 1993).

Carbon Dioxide

We tested two models for CO_2, the first was a two centre Lennard-Jones model originally due to Suzuki and Schnepp (1971) (SS) in which each site has Lennard-Jones parameters $\sigma = 0.29$ nm, $\varepsilon/k = 192.5$ K, and the site separation is $\ell = 0.23$ nm. The second model uses dispersion parameters due to McDonald et al. (1983). This model originally contained five point charges but was subsequently simplified for computational tractability by Hammonds et al. (1993) to three point charges but with the quadrupole moment unchanged. This model (which we shall term MOTHM) has Lennard-Jones (12-6) parameters $\sigma_{OO} = 0.3026$ nm, $\sigma_{CO} = 0.2925$ nm, $\sigma_{CC} = 0.2824$ nm, $\varepsilon_{OO}/k = 75.2$ K, $\varepsilon_{CO}/k = 44.5$ K, $\varepsilon_{CC}/k = 26.3$ K, and point charges on the atom centres of $q_O/e = -0.332$, $q_C/e = +0.664$. The O-O distance is 0.2324 nm and the C-O distance 0.1162 nm.

A spherical cutoff was used for carbon dioxide pair interactions with both the electrostatic and Lennard-Jones parts truncated at 2 nm. Because of the relatively large cutoff, no long range corrections were employed. We note that quadrupole-quadrupole interactions fall off as $1/r^5$, thus long range effects are less significant than for pair interactions between dipolar or charged species. The same cutoff condition was used for methane and nitrogen pair interactions (see below) and also for pair interactions between unlike species. The box side length was varied in order to ensure that sufficient particles remained in the simulation at each pressure, and was always greater than twice the cutoff distance. Periodic boundary conditions were applied in the usual way.

At a sufficiently large value of H, the potential fields from opposite walls of the pore do not overlap and each wall can be considered to be an isolated graphite surface at low coverages of the adsorbate. We used a value of $H = 10$ nm for this purpose. To facilitate comparison between simulation and experiment, it is important to recognise that volumetric adsorption measurements yield an adsorption excess, whilst simulations give the total number of particles in the system; to convert the raw simulation uptake data to an excess quantity, it is necessary to subtract from it the product of system volume and the bulk gas density (corresponding to a particular pressure). The "volume" used in this calculation needs to be the volume which is actually accessible to the carbon dioxide. We have discussed this question elsewhere (Kaneko et al., 1994), and define an accessible pore width H' for CO_2 by

$$H'(\text{nm}) = H(\text{nm}) - 0.24 \quad (10)$$

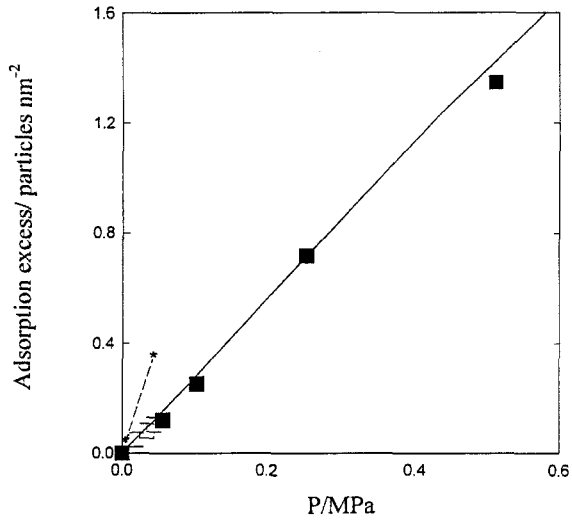

Figure 2. Comparison of experimental data for CO_2 adsorption on Vulcan 3G at 313.15 K with GCMC simulation for two potential models. Experiment: This work (■), Myers and Prausnitz (1965) (□). Simulation: MOTHM model (—), SS model (*-----*).

The comparison between simulation for the two models and experiment is shown in Fig. 2. In addition to the experimental data generated in this work, some results of Myers and Prausnitz (1965) are also shown. Although the two experimental data sets are in different pressure ranges, they can be seen to be mutually consistent. The simulation results using the MOTHM potential agree well with experiment, while those for the SS model do not; we have therefore adopted the MOTHM model for the remainder of this study. The figure shows the data over a limited range in order to highlight the differences between the two simulation models. The new experimental data are recorded in Table 1.

Table 1. Experimental results for CO_2 adsorbed on Vulcan 3G at 313.5 K.

Surface excess/nm^{-2}	Pressure/MPa
0.1205	0.0570
0.2528	0.1030
0.7166	0.2530
1.3469	0.5100
2.4456	1.0440
3.9081	2.0010
5.2094	3.0000
6.4361	3.9950
7.1288	4.5350

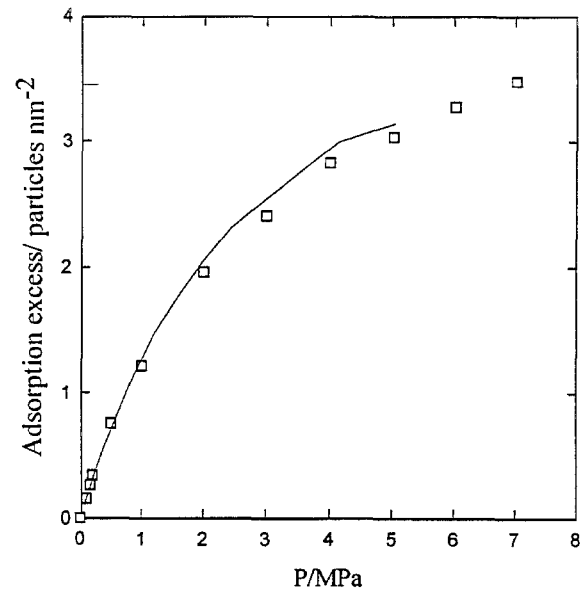

Figure 3. Comparison of experimental data for CH_4 adsorption on Vulcan 3G at 313.15 K from this work (□) with GCMC simulation (—) for a spherical Lennard-Jones model of CH_4.

Methane

Methane was modelled as a spherical Lennard-Jones particle with parameters; $\sigma_{CH_4} = 0.381$ nm, $\varepsilon_{CH_4}/k = 148.12$ K (Steele, 1974). An isotherm at 313.15 K for methane on a single graphite surface was simulated by GCMC and the raw simulation data converted to an excess using the method described above. A comparison between simulation and experimental measurements on Vulcan 3G is shown in Fig. 3; the agreement between simulation and experiment is sufficiently close to suggest that the methane model is satisfactory under these conditions.

Nitrogen

The model for nitrogen was based on that of Kuchta and Etters (1987). The dispersion and repulsive parts of the Kuchta-Etters potential for each site were parameterized to give a fit to a 12-6 Lennard-Jones potential (Freeman, 1993). The geometry of the model is shown in Fig. 4 with the quadrupole modelled as 4 point charges ($q = 0.373e$). The N-N separation is $\ell_{NN} = 0.1094$ nm and each N has Lennard-Jones parameters $\sigma_{NN} = 0.3318$ nm and $\varepsilon_{NN}/k = 37.8$ K. Simulated isotherms using this model have been previously tested against high pressure adsorption measurements for N_2

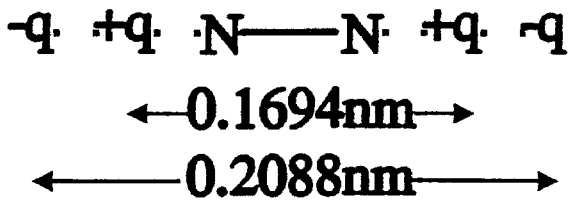

Figure 4. Model for N_2.

in well characterised active carbon fibres and extremely good agreement was obtained (Kaneko et al., 1994).

CO_2/CH_4 Mixtures

Figure 5 shows the variation of selectivity with bulk pressure for a CO_2/CH_4 mixture. A selectivity greater than unity indicates that CO_2 is more strongly adsorbed than CH_4. The bulk phase had equal partial fugacities for each gas, and for the pressure range studied this is approximately equivalent to having equal bulk mole fractions.

Selectivity increases monotonically with pressure for each pore size over the pressure range studied. This contrasts with simulation results for ethane/methane mixtures (Cracknell et al., 1994) and propane/ethane mixtures (Cracknell and Nicholson, 1994) for similar pore sizes over the same pressure range. In these hydrocarbon mixtures, either the selectivity initially increased with pressure to a maximum value and then decreased; or decreased monotonically with pressure. We have previously ascribed the rise in selectivity with pressure to a cooperative (energetic) adsorption effect and a decrease with pressure to an entropic effect whereby further adsorption necessitates increased ordering.

In the present case there is no maximum over the pressure range studied because the intermolecular interactions and hence the cooperative effects are much weaker in CO_2 than in ethane. Consequently the experimental CO_2 isotherm on a plane surface does not reach a plateau until about 35 bar compared to the ethane isotherm which saturates at about 10 bar. This means that ethane will be more tightly packed than CO_2 at these pressures and its rotational motions more restricted; a large part of the decrease in selectivity with pressure can be attributed to the loss in entropy associated with rotational restrictions.

It can be seen from Fig. 5 that selectivity has a rather complicated dependence on pore size; for example the pore of width $H = 0.8$ nm has the lowest selectivity at zero pressure of the three sizes shown; however from 0.5 bar to 1.5 bar it has the highest selectivity but from 17 bar onward the lowest selectivity again. Figure 6 shows selectivity versus pore size at pressures of $P = 0$

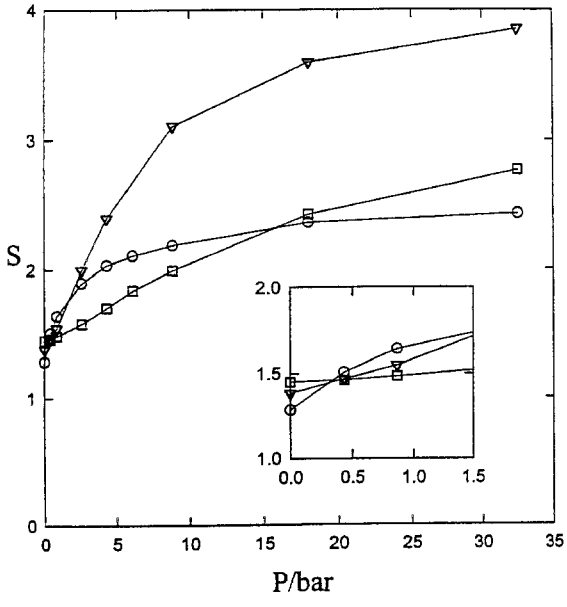

Figure 5. Selectivity versus pressure of CO_2 over CH_4 in pores of width, $H = 0.8$ nm (○), $H = 1.0$ nm (▽) and $H = 1.2$ nm (□) at 313.15 K. The gases have equal bulk partial fugacities (i.e., approximately equal bulk mole fractions).

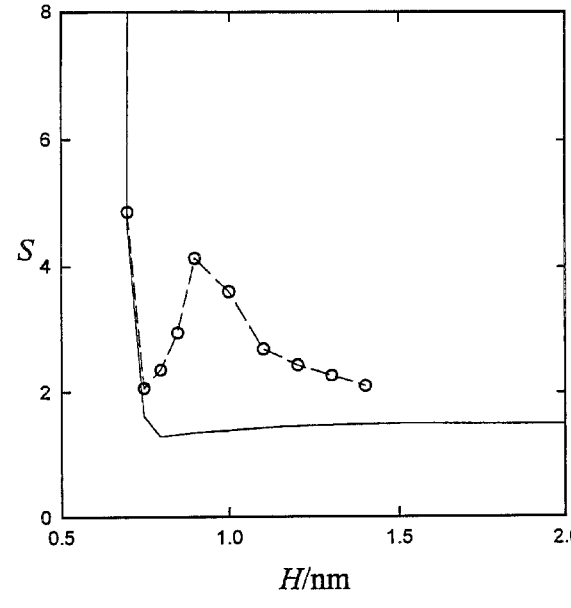

Figure 6. Selectivity of CO_2 over CH_4 at $P = 0$ bar (—) and $P = 18$ bar (–○–) as a function of pore width H at 313.15 K. The gases have equal bulk partial fugacities (i.e., approximately equal bulk mole fractions).

bar and $P = 18$ bar. In the limit of low pressure the selectivity (for a given H) was calculated from the ratio of the one particle partition functions,

$$S^0 = \frac{\frac{1}{4\pi}\int_V \exp\left(-\beta u_s^{\text{Carbon Dioxide}}(\boldsymbol{r}, \omega)\right) d\boldsymbol{r} d\omega}{\int_V \exp\left(-\beta u_s^{\text{Methane}}(\boldsymbol{r})\right) d\boldsymbol{r}} \quad (11)$$

Equation (11) was solved numerically using Monte Carlo integration with 10^7 trial points.

At both pressures, the selectivity of carbon dioxide over methane in the limit of small pore size is infinity. This contrasts with previous results for the ethane-methane system where the selectivity of ethane over methane goes to zero at the small pore size limit (Cracknell et al., 1994). In the direction normal to the C—C bond, ethane is approximately the same size as methane; thus for an internal pore size close to the smallest molecular diameter, ethane is constrained to lie parallel to the walls but there is no orientational restriction on methane (modelled as a spherical particle). It is therefore the reduction in ethane entropy which causes the selection of methane over ethane in the small pore limit because of the rotational confinement of the ethane. However the atoms in CO_2 with a σ of around 0.3 nm are much smaller in diameter than methane with $\sigma = 0.381$ nm. When H is small CO_2 molecules lying parallel to the walls are therefore energetically favoured compared to methane, despite the fact that rotational constraint lowers their entropy.

At both pressures shown in Fig. 6, the selectivity passes through a minimum at $H = 0.75$ nm. At zero pressure the selectivity rises monotonically to the right of this minimum, whilst for $P = 18$ bar the selectivity oscillates. To interpret these features, distribution functions (Fig. 7) and snapshots (Fig. 8) are shown for $P = 18$ bar. Note that in the snapshots shown in Fig. 8 methane is depicted as a grey sphere with a much smaller diameter than the van der Waals radius. Figure 7a shows the singlet density of methane as a function of distance, r, from the centre of the pore. It can be seen that at $H = 0.8$ nm, methane fits tightly into the pore, and this is an optimal packing energetically. This is the reason for the selectivity minimum at zero pressure in pores of this size seen in Fig. 6. The origin of the selectivity minimum at $H = 0.8$ nm for $P = 18$ bar is less easy to explain—it can be seen from Fig. 5 that the $H = 0.8$ nm pore actually has a higher selectivity than the $H = 1.0$ nm and $H = 1.2$ nm pores for certain pressures intermediate between 0 and 18 bar. As discussed above, selectivity-pressure relationships can be described in terms of a competing energetic cooperative adsorption effect and an entropic effect caused by the adsorbate having to order in a full pore—it is likely therefore that the selectivity minimum in the $H = 0.8$ nm pore at $P = 18$ bar, results from a combination of optimal packing for methane and an entropic penalty because CO_2 has to order itself in small pores. Figure 7b shows the singlet density of the position of the carbon atom in CO_2 at a pressure of 18 bar and Fig. 7c shows the orientation of the molecule relative to the normal to the pore walls. It can be seen that for $H = 0.8$ bar the CO_2 molecule either tends to lie flat against the wall (the shoulder in 7b) or with its oxygen atoms in the potential well of each wall and the carbon atom near to the centre of the pore. The average orientation for $H = 0.8$ nm when the carbon atom is at the pore centre suggests that the CO_2 is indeed rotationally hindered, since the maximum value of $\langle \cos^2 \theta \rangle$ is only 0.4. The snapshot for $H = 0.8$ nm and $P = 18$ bar (Fig. 8a) confirms this.

The selectivity for $P = 18$ bar goes through a maximum at $H = 0.9$ nm. This occurs for two reasons: Firstly methane can no longer pack optimally (Fig. 7a) since there is insufficient room for two layers, yet too much room for just one. Secondly, CO_2 is no longer orientationally hindered as can be seen in the snapshot (Fig. 8b) where CO_2 molecules either span the pore or lie flat against one wall. The pore size is therefore entropically favoured relative to $H = 0.8$ nm. The proportion of CO_2 spanning the pore at $H = 0.9$ nm can be seen from Fig. 7b to be less than the number lying flat against the wall. It is slightly more favourable energetically for the molecule to lie flat because the carbon atom is in the potential minimum as well as the two oxygens. This contrasts with the behaviour of ethane, modelled as two Lennard-Jones methyl groups (Cracknell et al., 1994), where lying flat or spanning the pore were isoenergetic configurations.

At $H = 1.0$ nm, it can be deduced from Figs. 7b, 7c and 8c that the CO_2 can now pack into two layers but must lie flat against the pore wall in order to do so. This is entropically unfavourable relative to the $H = 0.9$ nm pore but energetically favourable since the carbon atoms can remain in the potential minima. At $H = 1.2$ nm the structure of the adsorbed phase is more disordered with CO_2 molecules either lying flat on each wall or lying parallel to it; the angle profile (Fig. 7c) shows a maximum corresponding to molecules attached to the walls by one atom and a minimum in the pore centre.

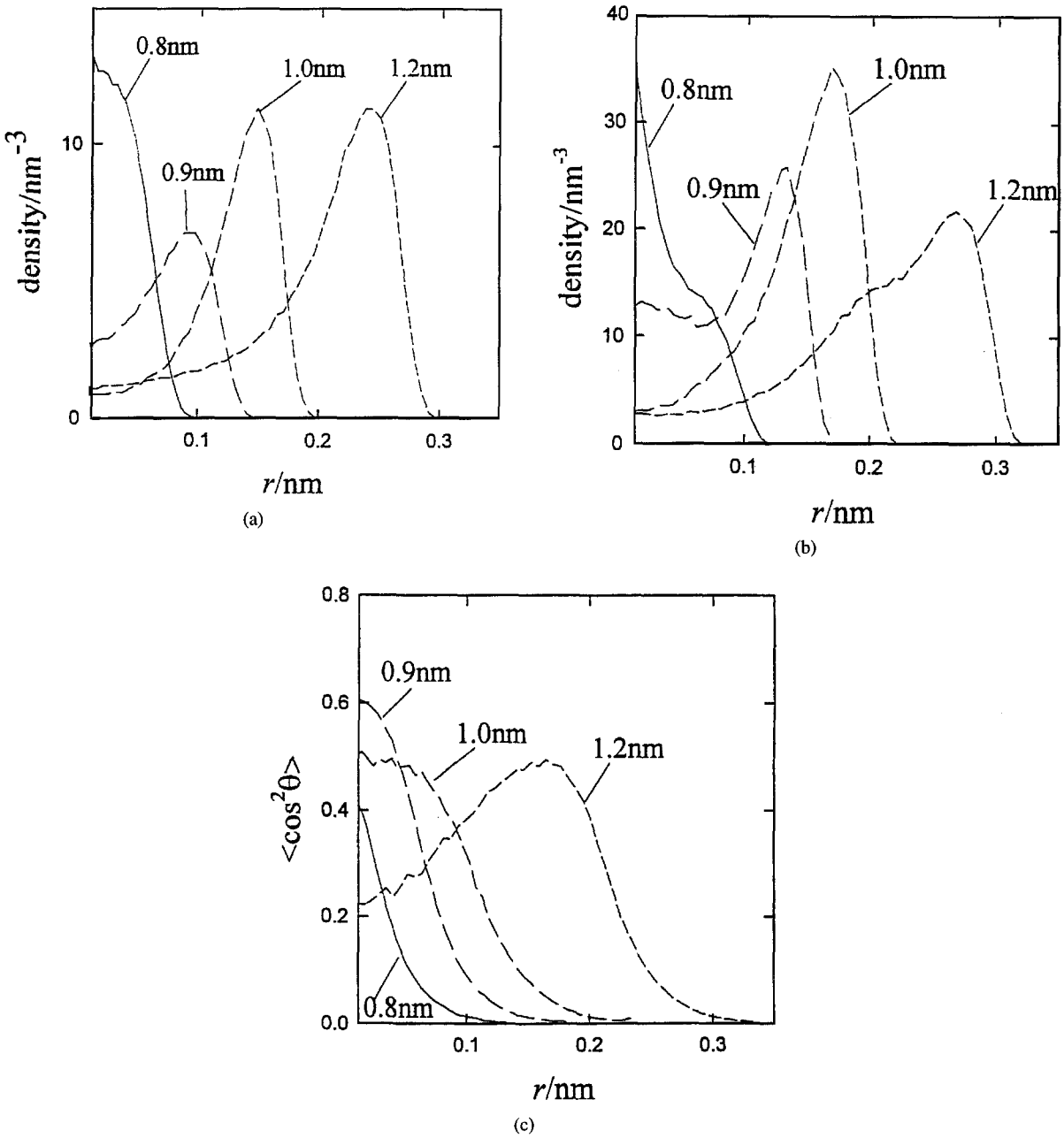

Figure 7. Distribution functions at $P = 18$ bar and 313.15 K for pores of width $H = 0.8$ nm, $H = 0.9$ nm, $H = 1.0$ nm and $H = 1.2$ nm for gases with equal partial bulk fugacities (a) singlet density of methane as a function of distance from pore centre, (b) singlet density of carbon atom on CO_2, angular distribution function, $\langle \cos^2 \theta \rangle$, for CO_2 where θ is the angle between the CO_2 and the normal to a pore wall.

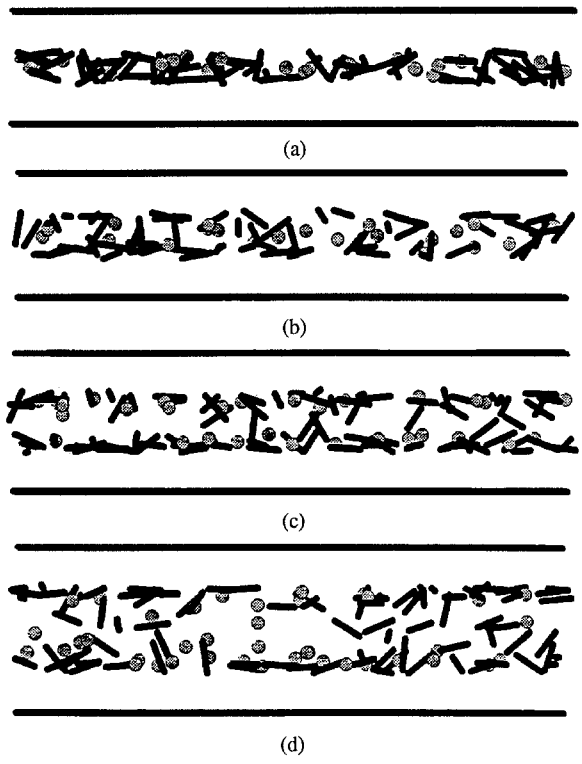

Figure 8. Snapshots for CO_2 and methane at $P = 18$ bar and 313.15 K for gases with equal partial gas fugacities in pores of width (a) $H = 0.8$ nm, (b) 0.9 nm, (c) $H = 1.0$ nm and (d) 1.2 nm. The C—O—C axis is shown as a black line, while methane is shown as a grey sphere of radius less than the Van der Waals radius.

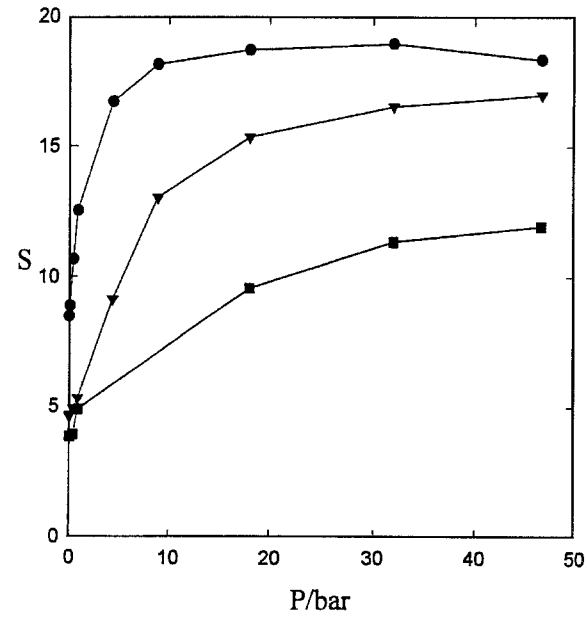

Figure 9. Selectivity verses pressure of CO_2 over N_2 in pores of width, $H = 0.8$ nm (●), $H = 1.0$ nm (▼) and $H = 1.2$ nm (■) at 313.15 K. The gases have equal bulk partial fugacities (i.e., approximately equal bulk mole fractions).

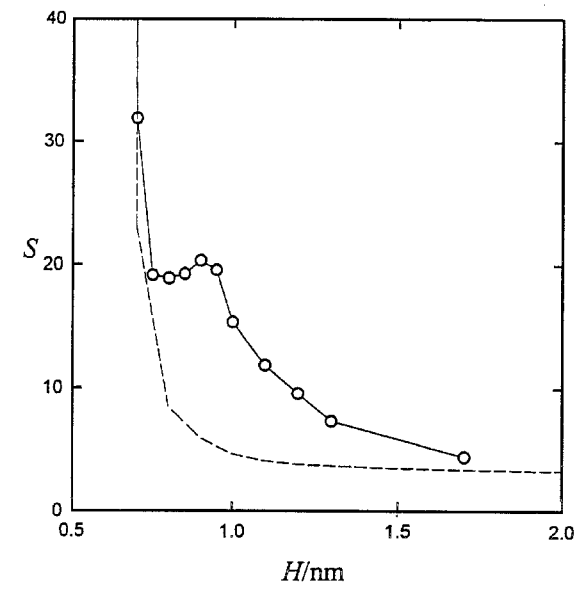

Figure 10. Selectivity of CO_2 over N_2 at $P = 0$ bar (——) and $P =$ 17.7 bar (–○–) as a function of pore width H at 313.15 K. The gases have equal bulk partial fugacities (i.e., approximately equal bulk mole fractions).

CO_2/N_2 Mixtures

Figure 9 shows pressure-selectivity relationships for $H = 0.8$ nm, $H = 1.0$ nm and $H = 1.2$ nm for CO_2 and N_2. The bulk gas has equal partial fugacities of each component which, to a good approximation, for the pressure range studied, is equivalent to having equal bulk mole fractions. The temperature is 313.15 K. A selectivity greater than unity indicates that CO_2 is selectively adsorbed over N_2. The selectivity increases with pressure over the range 0–45 bar for the two larger pores. There is evidence of a maximum for the smaller pore attributable to an entropic effect. At all the pressures studied the $H = 0.8$ nm pore has a larger selectivity than the $H = 1.0$ nm pore which has a larger selectivity than the $H = 1.2$ nm pore. That the selectivity for CO_2 over N_2 is in general higher than over CH_4 reflects the fact that N_2 adsorbs less strongly than CH_4.

Figure 10 shows the relationship between selectivity and pore size at 0 bar and 17.7 bar for the CO_2/N_2 system. At the limit of small pore size the selectivity of CO_2 over N_2 goes to infinity. As for the CO_2/CH_4 mixtures, this occurs because the CO_2 molecule has a rather smaller diameter around its axis than nitrogen

($\sigma = 0.3$ nm compared to $\sigma = 0.332$ nm), it therefore experiences a strong attraction in pores which are repulsive to nitrogen. It is important to stress that these conclusion about the zero pressure limiting selectivity are likely to depend significantly on the models used for the adsorptives. Although these have been shown to provide accurate representations of adsorption on a single graphite surface, this does not mean that they are perfect. The zero pressure selectivity, decreases monotonically with pore size; the packing effect giving rise to a minimum for the CO_2/CH_4 system being absent in this case. The curve for $P = 17.7$ bar shows a small minimum at 0.8 nm and a maximum at 0.9 nm. The minimum in the 0.8 nm pore is shallower than that in the CO_2/CH_4 system, and so the selectivity at 0.8 nm is still higher than at $H = 1.0$ nm and 1.2 nm as shown in Fig. 9.

Figure 11 shows snapshots in pores of width 0.8 nm (a), 1.0 nm (b) and 1.2 nm (c), at a pressure of 17.7 bar for CO_2/N_2 mixtures at 313.15 K with equal bulk gas fugacities. As was also observed in Fig. 7c, a pore of width $H = 0.8$ nm does rotationally hinder the CO_2 but does not rotationally hinder the N_2 to the same extent, since the molecule is shorter. The minimum can therefore be ascribed to an entropic effect. As the pore gets wider, CO_2 ceases to be rotationally hindered and the selectivity increases slightly.

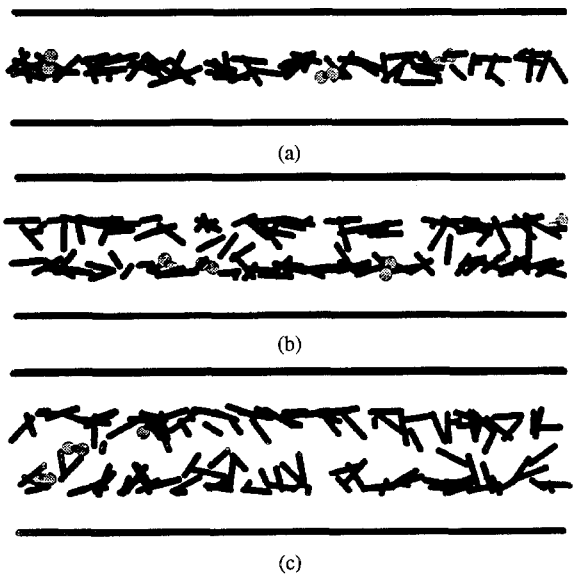

Figure 11. Snapshots for CO_2 and N_2 at $P = 17.7$ bar and 313.15 K for gases with equal partial gas fugacities in pores of width $H = 0.8$ nm (a), $H = 1.0$ nm (b) and $H = 1.2$ nm (c). The C—O—C axis is shown as a black line and N_2 is shown as a black line joining grey spheres (of radius less than the Van der Waals radius on the N atoms).

Conclusions

New experimental results employing a high pressure rig, are reported for the adsorption of CO_2 on non-porous vulcan. Simulations using the model of Hammonds et al. (1990), together with the 10-4-3 adsorbate-adsorbent potential, give an accurate account of the experimental results at ambient temperatures. The potential models used here for methane and nitrogen have also been validated under similar conditions.

Mixture simulations demonstrate that carbon dioxide is selectively adsorbed from equimolar mixtures in preference to both methane and nitrogen in slit shaped model carbon pores at ambient temperatures, in agreement with preliminary experimental results for these mixtures in microporous carbonaceous membrane materials (Bromhead and Tennison, to be published). In very small pores with a physical width below 0.7 nm, which corresponds to an internal width of less than ~0.5 nm, methane or nitrogen is virtually excluded compared to CO_2. This is a sieving effect which is of course highly dependent on the molecular models employed in the simulations and may not be realisable in practice, since it is dependent on the CO_2 entering the pores with its axis nearly parallel to the pore wall. In pores larger than this, selectivities are rather low (less than 4) for the methane mixtures, but nearly an order of magnitude higher for the less strongly adsorbed nitrogen. The high selectivity at low pore widths and the apparent absence of a pressure maximum in selectivity, distinguish the CO_2 mixtures from the previously studied hydrocarbon mixtures (Cracknell et al., 1994; Cracknell and Nicholson, 1994). The latter observation is explained by an interplay of energetic effects—leading to a more gradual saturation of the CO_2 isotherm—and entropy effects. In common with this previous work the present study again reveals the complex interaction between packing, energetic and entropic factors which can control selective behaviour in small pores.

Acknowledgments

We wish to thank the CEC for a grant (BRITE EURAM CONTRACT BREU-CT92-0568) in support of this work; one of us (DN) wishes to thank NATO for a travel grant.

References

Allen, M.P. and D.J. Tildesley, *Computer Simulation of Liquids*, Clarendon, Oxford, U.K., 1987.

Cracknell, R.F., D. Nicholson, and N. Quirke, "A Grand Canonical Study of Lennard-Jones Mixtures in Slit Shaped Pores," *Molec. Phys.*, **80**, 885–897 (1993).

Cracknell, R.F. and D. Nicholson, "Grand Canonical Study of Lennard-Jones Mixtures in Slit Pores. Part 3—Mixtures of Two Molecular Fluids: Ethane and Propane," *J. Chem. Soc. Faraday Trans.*, **90**, 1487–1493 (1994).

Cracknell, R.F., D. Nicholson, and N. Quirke, "Grand Canonical Study of Lennard-Jones Mixtures in Slit Pores. 2: Mixtures of Two-Center Ethane with Methane," *Molec. Sim.*, **13**, 161–173 (1994).

Cracknell, R.F. and D. Nicholson, "Adsorption of Gas Mixtures on Solid Surfaces, Theory and Computer Simulation," *Adsorption*, **1**, 7–16 (1995).

Everett, D.H., G.D. Parfitt, K.S.W. Sing, and R. Wilson, *J. Appl. Chem. Biotechnol.*, **24**, 199 (1974).

Freeman, N.A., Ph.D. Thesis, London University (1993).

Hammonds, K.D., I.R. McDonald, and D.J. Tildesley, "Computational Studies of the Structure of Carbon Dioxide Monolayers Physisorbed on the Basal Plane of Graphite," *Molec. Phys.*, **70**, 175–195 (1990).

Hammonds, K.D., I.R. McDonald, and D.J. Tildesley, "Computational Studies of the Structure of Monolayers of Chlorine Physisorbed on the Basal Plane of Graphite," *Molec. Phys.*, **78**, 173–189 (1993).

Jiang, S., P.B. Balbuena, and K.E. Gubbins, "Theory of Adsorption of Trace Compounds," *J. Phys. Chem.*, **98**, 2403–2411 (1994).

Joseph, J.C., A.L. Myers, T.C. Golden, and S. Sircar, "Adsorption of Trace Gases (Propane, Butane and Freon 12) from Carrier Gases (Helium, Nitrogen and Carbon Dioxide) on Activated Carbon," *J. Chem. Soc. Faraday Trans.*, **89**, 3491–3497 (1993).

Kaminsky, R.D. and P.A. Monson, "Modelling of the Influence of Heterogeneous Adsorbent Microstructure upon Adsorption Equilibrium for Binary Mixtures," *Langmuir*, **10**, 530–537 (1994).

Kaneko, K., S. Shimizu, and T. Suzuki, "Intra-Pore Field Dependent Micropore Filling of Supercritical N_2 in Slit-shaped Micropores," *J. Chem. Phys.*, **97**, 8705–8711 (1992).

Kaneko, K., R.F. Cracknell, and D. Nicholson, "Nitrogen Adsorption in Slit Pores at Ambient Temperatures: Comparison of Adsorption and Experiment," *Langmuir*, **10**, 4606–4609 (1994).

Karavias, F. and A.L. Myers, "Monte Carlo Simulation of Binary Gas Adsorption in Zeolite Cavities," *Mol. Sim.*, **8**, 51–72 (1991).

Keller, G.E., "Gas Adsorption Processes—State of the Art," *Industrial Gas Separations*, T.E. Whyte, C.M. Yon, and E.H. Wagener (Eds.), ACS Symposium Series No. 223, 145–169 (1985)

Kierlik, E. and M.L. Rosinberg, "Density Functional Theory for Inhomogeneous Fluids: II Adsorption of Binary Mixtures," *Phys. Rev. A*, **44**, 5025–5037 (1991).

Kofke, D.A. "Solid-Fluid Coexistence in Binary Hard Sphere Mixtures by Semigrand Monte Carlo Simulation," *Molec. Sim.*, **7**, 285–302 (1991).

Kuchta, B. and R.D. Etters, "Calculated Properties of Monolayer and Multilayer N_2 on Graphite," *Phys. Rev. B.*, **36**, 3400–3406 (1987).

Maddox, M.W. and J.S. Rowlinson, "Computer Simulation of a Fluid Mixture in Zeolite Y," *J. Chem. Soc. Faraday Trans.*, **89**, 3619–3621 (1993).

Murthy, C.S., S.F. O'Shea, and I.R. McDonald, "Electrostatic Interactions in Molecular Crystals: Lattice Dynamics of Solid Nitrogen and Carbon Dioxide," *Molec. Phys.*, **50**, 531 (1983).

Myers, A.L. and J.M. Prausnitz, "Thermodynamics of Mixed Gas Adsorption," *AIChE J.*, **11**, 121–126 (1965).

Myers, A.L. and J.M. Prausnitz, "Hindered Rotation in Physical Adsorption," *Trans. Faraday Soc.*, **61**, 755–771 (1965).

Nicholson, D. and N.G. Parsonage, *Computer Simulation and the Statistical Mechanics of Adsorption*, Academic, New York, U.S.A. 1982.

Razmus, D.M. and C.K. Hall, "Prediction of Gas Adsorption in 5A Zeolites Using Monte Carlo Simulation," *AIChE J.*, **37**, 769–775 (1991).

Somers, S.A., A.V. McCormick, and H.T. Davis, "Modelling the Influence of Heterogeneous Adsorbent Microstructure," *J. Chem. Phys.*, **99**, 9890–9908 (1993).

Steele, W.A., *The Interaction of Gases with Solid Surfaces*, Pergamon, Oxford, U.K., 1974.

Suzuki, M. and O. Schnepp, "Intermolecular Potential and Lattice Dynamics of the CO_2 Crystal," *J. Chem. Phys.*, **55**, 5349–5356 (1971).

Tan, Z., U.M.B. Marconi, F. van Swol, and K.E. Gubbins, "Hard Sphere Mixtures Near a Hard Wall," *J. Chem. Phys.*, **90**, 3704–3712 (1989).

Tan, Z. and K.E. Gubbins, "Selective Adsorption of Simple Mixtures in Slit Pores: A Model of Methane-Ethane Mixtures in Carbon," *J. Phys. Chem.*, **96**, 845–854 (1992).

Van Tassel, P.R., H.T. Davis, and A.V. McCormick, "Adsorption Simulations of Small Molecules and their Mixtures in a Zeolite Micropore," *Langmuir*, **10**, 1257–1267 (1994).